An Energy-efficient and Lightweight Indoor Localization System for Internet-of-Things (IoT) Environments

MYEONGCHEOL KWAK, Seoul National University, Republic of Korea
YOUNGMONG PARK, Hubilon Co., Ltd., Republic of Korea
JUNYOUNG KIM, SK Telecom Co., Ltd., Republic of Korea
JINYOUNG HAN, Hanyang University, Republic of Korea
TAEKYOUNG KWON, Seoul National University, Republic of Korea

Each and every spatial point in an indoor space has its own distinct and stable fingerprint, which arises owing to the distortion of the magnetic field induced by the surrounding steel and iron structures. This phenomenon makes many indoor positioning techniques rely on the magnetic field as an important source of localization. Most of the existing studies, however, have leveraged smartphones that have a relatively high computational power and many sensors. Thus, their algorithmic complexity is usually high, especially for commercial location-based services. In this paper, we present an energy-efficient and lightweight system that utilizes the magnetic field for indoor positioning in Internet of Things (IoT) environments. We propose a new hardware design of an IoT device that has a BLE interface and two sensors (magnetometer and accelerometer), with the lifetime of one year when using a coin-size battery. We further propose an augmented particle filter framework that features a robust motion model and a localization heuristic with small sensory data. The prototype-based evaluation shows that the proposed system achieves a median accuracy of 1.62 m for an office building, while exhibiting low computational complexity and high energy efficiency.

CCS Concepts: • **Human-centered computing** → **Ubiquitous and mobile computing**; • **Hardware** → *Sensor devices and platforms*;

Additional Key Words and Phrases: Particle Filter, Internet-of-Things, Magnetic Field, Wireless Communication, Indoor Localization, BLE

ACM Reference Format:
Myeongcheol Kwak, Youngmong Park, Junyoung Kim, Jinyoung Han, and Taekyoung Kwon. 2018. An Energy-efficient and Lightweight Indoor Localization System for Internet-of-Things (IoT) Environments. *Proc. ACM Interact. Mob. Wearable Ubiquitous Technol.* 2, 1, Article 17 (March 2018), 28 pages. https://doi.org/10.1145/3191749

This work was supported in part by the Ministry of Education of the Republic of Korea and the National Research Foundation of Korea (NRF-2017S1A5B8058870). Both the snu-samsung smart campus research center and the ICT at Seoul National University provides in part research facilities for this study.
Corresponding Authors: Jinyoung Han (jinyounghan@hanyang.ac.kr) and Taekyoung Kwon (tkkwon@snu.ac.kr).
Authors' addresses: Myeongcheol Kwak, Seoul National University, 138-414, 1 Gwanak-ro, Gwanak-gu, Seoul, 08826, Republic of Korea; Youngmong Park, Hubilon Co., Ltd. Namgang 5F, 291, Gangnam-daero, Seocho-gu, Seoul, 06729, Republic of Korea; Junyoung Kim, SK Telecom Co., Ltd. SKT IoT Tech. Lab, 246 Hwangsaeul-ro, Bundang-gu, Seongnam, Gyeonggi, 13595, Republic of Korea; Jinyoung Han, Hanyang University, 55 Hanyangdaehak-ro, Sangnok-gu, Ansan, Gyeonggi, 15588, Republic of Korea; Taekyoung Kwon, Seoul National University, 301-503, 1 Gwanak-ro, Gwanak-gu, Seoul, 08826, Republic of Korea.

2474-9567/2018/3-ART17 $15.00
https://doi.org/10.1145/3191749

1 INTRODUCTION

Location-based applications such as car navigation systems, restaurant recommendation systems, parking locators, and emergency escape services have significantly increased the quality of our daily life. The location of a user is key contextual information that is utilized by such location-based services (LBSs) [47]. However, in indoor environments, the location of a user cannot be easily acquired owing to the blockade of global positioning system (GPS) signals by building structures. Hence, over the last decade, many methods for indoor localization have been proposed.

There have been many attempts to use various sources of information for indoor localization. Methods that utilize WiFi signals [2, 6, 39] are among the most widely used ones. However, these methods require frequent WiFi scans that result in signification consumption of energy. In addition, fluctuations in the signal strength negatively affect the localization performance. Ultra-wideband (UWB) based methods [13, 34, 40] can be highly accurate. However, these methods require customized hardware devices for analyzing reflected signals. More practical solutions are based on inertial sensors including magnetometers, accelerometers, and gyroscopes [25]. However, these solutions have their own limitations. For instance, a heading inference mechanism in pedestrian dead reckoning (PDR) [3] usually suffers from the distortion effect of steel materials on geo-magnetism.

The distortion effect of steel materials on a magnetic field is a double-edged sword. Since the magnetic distortion makes each spatial point distinct from others, it can serve as a fingerprint that helps localize any device with a magnetic sensor. As claimed in [14] and [32], magnetic fields exhibit desirable properties for indoor localization, e.g., temporal stability and insensitivity to moving nearby objects [26]. In addition, magnetic sensors are cheap and off-the-shelf everywhere. Consequently, many studies have proposed to use magnetic fields to a certain degree: a complete system [26, 37], a supplementary module [27, 38, 43], or a combination with other sources [10, 19].

The main problem associated with using magnetic fields for fingerprinting is that their sensor data requires special processing. The raw sensor reading from a magnetometer is parameterized as a three-dimensional vector, which should be transformed to a scalar (i.e., the magnitude of the vector) or to a two-dimensional vector [17], to mitigate the effect of noise owing to the device's movement. Note that such movement affects the reference coordinates, not the magnetic field itself. To deal with this issue, Maloc [37] and Magicol [26] used a temporal change in the magnetic field (generated in the course of the user's motion) as a fingerprint, and incorporated this measure into a particle filter framework. However, comparison of the temporal patterns of the magnetic field and processing of the particle filter technique is computationally expensive, and is feasible only with high-end devices such as smartphones. In other words, such solutions may not be used for low-end devices such as Internet of things (IoT) devices, unless the issues of high computation complexity and energy efficiency are resolved. An energy-efficient and lightweight indoor localization technique is essential for IoT device-based localization.

IoT devices are typically small, lightweight, and energy-efficient, and thus are easy to deploy or relocate, compared with smartphones or other dedicated localization devices (i.e., foot-mounted IMUs). If the performance of IoT device-based localization is sufficient for commercial-grade service, it can be a low-cost and energy-efficient alternative for many LBSs: supervising and tracking of assets and employees in office/factory environments, preventing workers from entering hazard zones, providing more precise geofencing services for patients or child care, and guiding emergency escape, to name a few.

To address these constraints and to reduce the cost of computation, we propose a novel magnetic field-based indoor localization system for IoT devices. We use energy saving wireless communication, bluetooth low energy (BLE), and report here a proprietary system that features a BLE interface and a magnetic sensor. We also streamline the positioning algorithms to reduce the computational complexity while maintaining the localization accuracy. In summary, our work makes the following contributions.

- To the best of our knowledge, this paper is the first attempt to design a magnetic field-based, energy-efficient, and lightweight indoor localization system for IoT applications. The first-class requirement for IoT devices

is energy efficiency; hence, we tackle the algorithmic complexity and energy efficiency while maintaining the localization precision.
- In this work, we develop a specialized IoT device hardware (and the corresponding firmware) that substantiates energy-efficient localization (Section 4).
- To reduce the system complexity, we streamline the server-side localization algorithms, as well as the design of the end-user device, while maintaining localization performance comparable to those of state-of-the-art localization techniques (Section 5).
- Using sensor data that had been collected over a period of three months, we demonstrate that our proposed system is energy-efficient, i.e., a single-coin battery can last for one year.

This paper is organized as follows. After reviewing some related work in Section 2, we discuss several issues associated with the use of magnetic fields in Section 3. In Section 4, we explain our design of an IoT device for magnetic field-based localization. Section 5 introduces the architecture of our system that supports energy-efficient and lightweight localization for IoT environments. We then evaluate the proposed system in Section 6. After discussing practical issues in Section 7, we conclude the paper in Section 8.

2 RELATED WORK

Over the last decade, many efforts have been made to utilize distortion of the magnetic field in an indoor environment for localization. [33] first exploited the disturbance of a magnetic compass reading for positioning of a robot subject to some constraints. [8, 12, 35] attempted to leverage raw magnetic field data to construct a magnetic fingerprint. However, the raw magnetic field data significantly change with the location and heading of a magnetic sensor. These techniques thus require magnetic sensors to be fixed in space, or require a high overhead of the site survey or wardriving. These limitations make it difficult to use these approaches for positioning of humans. Therefore, as argued in [32] and [17], the raw magnetic field data should be transformed to make the sensor data robust to changes in the sensor's position as the users move. [32] and [15] proposed a magnetic fingerprinting scheme based on the magnetic field's intensity, which is a scalar. However, these systems can only localize users that move in straight trajectories, such as corridors; they cannot be used in complex structured areas. The systems proposed in MaLoc [37] and Magicol [26] adopted a two-dimensional magnetic fingerprinting model suggested in [17]. As the variation in the magnetic field data increases, the corresponding location is more likely to be uniquely identified, which enhances the localization performance. They also chose a particle filter framework to adapt to the complexity of indoor environments. However, the adoption of the particle filter framework significantly increases the algorithmic complexity of the problem, which reduces the device's energy efficiency. We believe that methods to reduce the cost of the site survey and to reduce the complexity of the system's operation (e.g., dynamic time warping (DTW) [4]) have not been given due attention; this realization motivated us to design a proprietary system for commercial-grade services.

3 ISSUES ON USING MAGNETIC FIELD

3.1 Characteristics of Magnetic Field

As claimed in [14], approaches that use sensory data and radio frequency (RF) signals for indoor localization should have three desirable properties: time-invariance, spatial distinctiveness, and universality. The sensory data generated by magnetic fields have been accepted to have these properties [1, 32, 37]. In addition, these magnetic fields are not affected by human bodies or moving (non-metal) objects in indoor environments [26]. This is one of the outstanding advantages of using magnetic fields for indoor localization, compared with varying RF signals such as WiFi.

Moreover, as explained in the previous section, the sensor data should be transformed to enhance the method's robustness with respect to changes in the position and heading of a magnetic sensor. The raw magnetic field data

are parameterized as a three-dimensional vector, $B_{raw} = (B_x, B_y, B_z)$. As suggested in [17], it is possible to obtain a two-dimensional vector B_{hv} that consists of the horizontal component B_h and the vertical component B_v by rotating B_{raw} onto a gravity plane. Note that B_{hv} is hardly changed even if a magnetic sensor changes its position or heading due to a movement (e.g., the sensor holder's movement). That is why this transformation process is crucial when using the magnetic field for localization. While a two-dimensional vector form of a magnetic field for each spatial point is very helpful, it may not be sufficient for fine-grained localization, compared with WiFi fingerprinting that can be very high-dimensional. To overcome this phenomenon, [26] suggested to add another dimension to B_{hv} by accumulating the temporal history of B_{hv}, and use the temporal vector of B_{hv} as a magnetic fingerprint. We adopted the same approach in this paper.

3.2 Variation Issues

Even if the magnetic field in indoor environments is stable, actual sensor readings are somewhat complicated, owing to several reasons. First, different magnetic sensors at the same location may show different readings, which can be owing to different manufacturing materials and/or different sensing mechanisms in these magnetic sensors. Figure 1(a) shows the magnetic sensor readings from three different devices over the same corridor (length, 60 m). Note that we plot only B_v for the sake of simplicity. The absolute differences between the readings of the three devices vary substantially, but their patterns of signal changes are similar. We can confirm this phenomenon by applying the mean removal technique to the individual patterns, as shown in Figure 1(b). The tendencies along the same trajectory can be slightly different if the heights of the magnetic sensors (i.e., their altitude from the floor) are different, but this difference is not substantial (see [37]).

Second, even the same magnetic sensors may exhibit different readings owing to a possible bias associated with the ferromagnetic materials, which results from the previous magnetic readings. Figure 2(a) shows the magnetic sensor readings for the same magnetic sensor, at different distances from a ferromagnetic material (i.e., a battery). It shows the patterns of B_v along the same corridor as the distance varies between the sensor and the ferromagnetic material (1, 2, and 3 cm). The absolute difference increases as the magnetic disturbance increases, but again, the trends of signal change are similar (compare with Figure 1(b)). Thus, the signal differences owing to this bias can also be removed by applying the mean removal technique, as shown in Figure 2(b). Note that we also adopted here the ellipsoid-fitting calibration method [22] that can compensate the bias itself with a simple swinging gesture.

Third, for the same trajectory, different walking speeds of different users will result in different rates of changes in magnetic readings. Figure 3 shows the magnetic fingerprints of users moving at different speeds along the same trajectory. The rates of change in the magnetic data are different while the patterns of signals in the two plots are similar. This phenomenon may make the location finding/matching process somewhat more difficult. To address this issue, [26] leveraged the DTW algorithm [4]. The DTW algorithm allows to compare two sequences with different time scales or speeds. However, its complexity is so high that using the particle filter framework may demand many more system resources. Thus, in our approach we aimed to avoid using the DTW algorithm.

3.3 Sensing Rate

The rate of reading of a magnetic sensor is directly related to the amount of data to process. It decides not only how frequently the magnetic field data are acquired, but also how much of the device's energy is consumed. Thus, choosing the right sensing rate is important, especially considering the IoT paradigm. Recent smartphones can choose the sensing frequency in the range from dozens to hundreds Hz. As we seek to reduce the devices' energy consumption, we set the sensing rate to be as small as possible. Figure 4 shows the magnetic fingerprints for different sensing rates, for users walking at normal speeds. Compared with the fingerprint pattern for the 50 Hz sensing rate in Figure 4(a), the pattern for the 3 Hz sensing rate in Figure 4(b) exhibits almost no loss. Note that

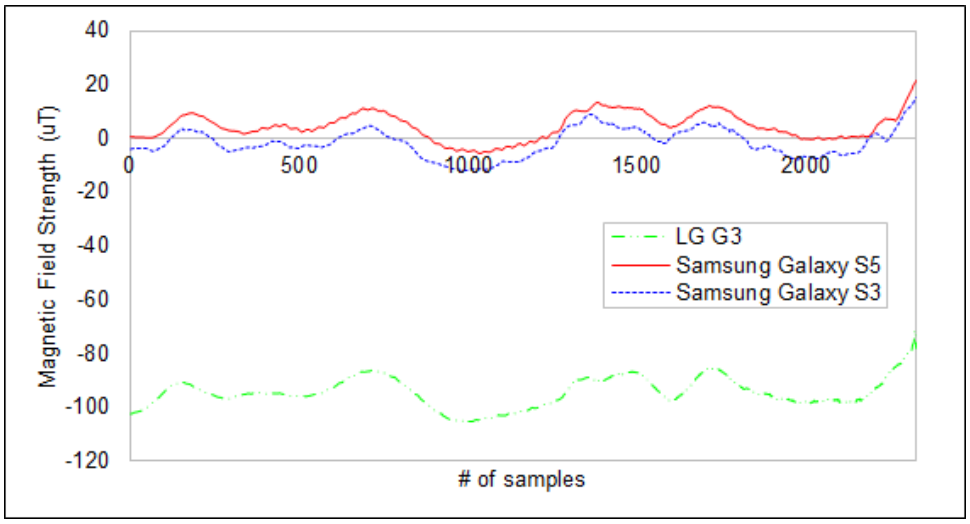

(a) before mean removal

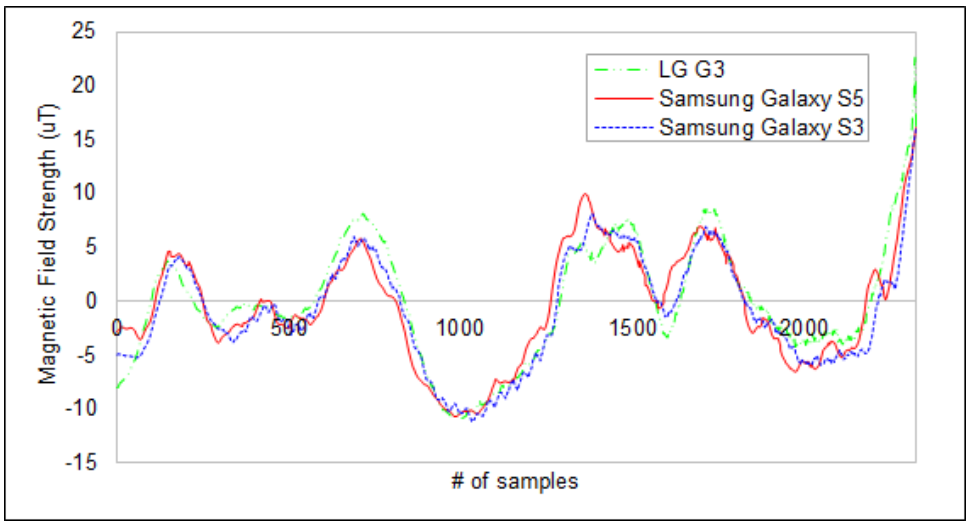

(b) after mean removal

Fig. 1. Sensor readings from different magnetic sensors are plotted before and after mean removal, which shows that the relative change in magnetic readings along the trajectory is independent of magnetic sensors.

the fingerprint for the 1 Hz sampling rate in Figure 4(c) reveals some pattern losses, especially at the beginning and the end of the trajectory. We also plot the fingerprint for the 0.5 Hz sampling rate in Figure 4(d), which shows many pattern losses overall. We thus chose 3 Hz as the sensing rate.

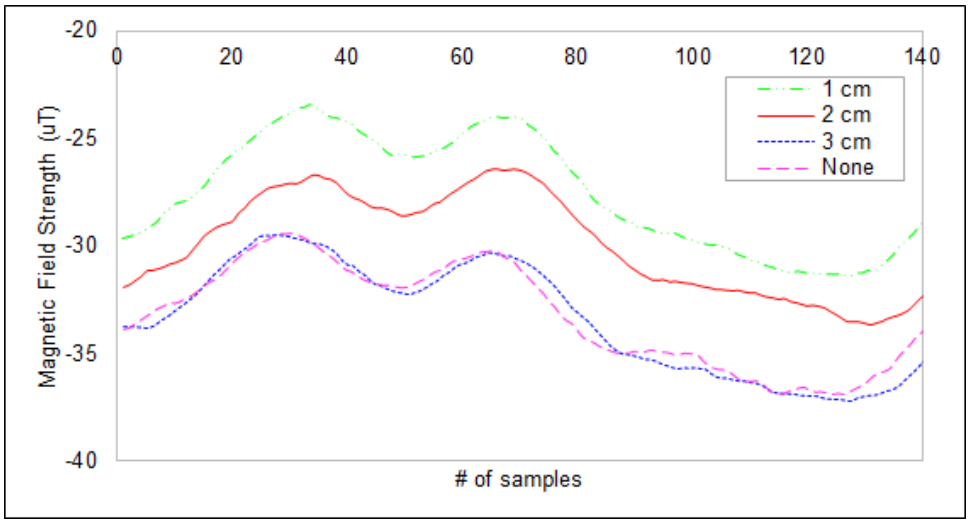

(a) before mean removal

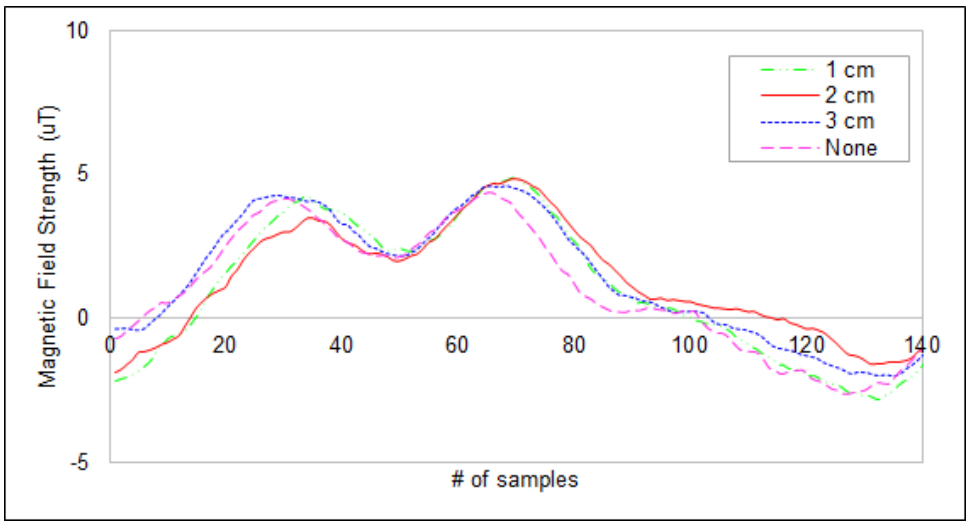

(b) after mean removal

Fig. 2. Sensor readings from the same magnetic sensor are plotted before and after the mean removal, as the distance from the ferromagnetic material varies.

4 DESIGN OF ENERGY-EFFICIENT DEVICE FOR LOCALIZATION

Considering the observations and issues, we now introduce the design of an IoT device for magnetic field-based localization.

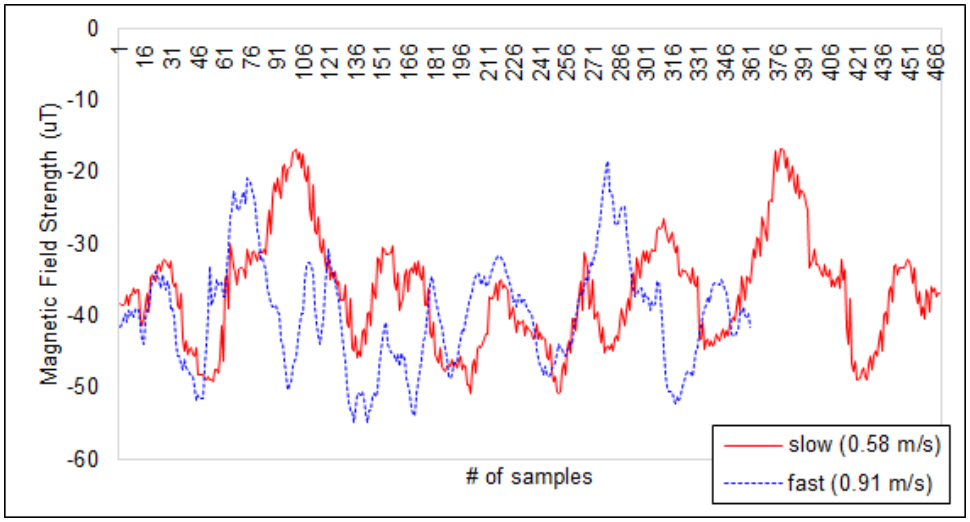

Fig. 3. Sensor readings for users moving at different speeds.

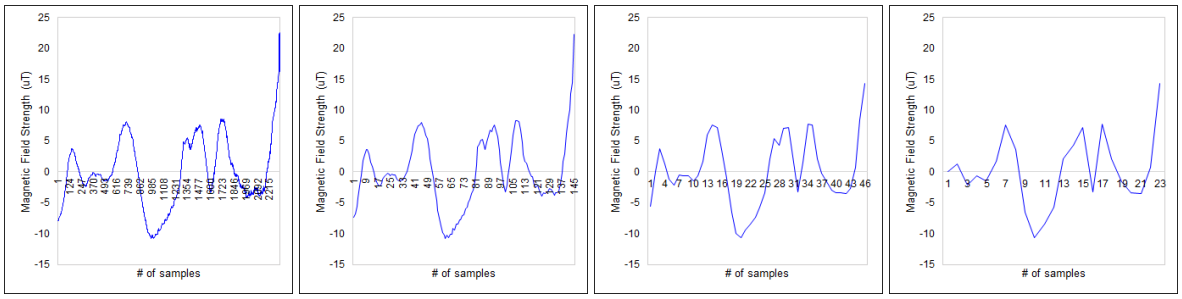

(a) 50Hz (b) 3Hz (c) 1Hz (d) 0.5Hz

Fig. 4. Magnetic fingerprints obtained in the same corridor, for different sensing rates. Sensing rates as low as 3 Hz yield only marginal information loss.

4.1 Hardware Design

We aim to build a positioning system that uses IoT devices in office areas, in cooperation with SK Telecom [31], a leading mobile operator in South Korea. Among candidate platforms for IoT devices, we chose a small ID card, to which positioning functionalities were added. Figure 5 shows an ID card (right) in the size of a credit card, and a sensor-equipped board (left), in which the positioning functionalities were implemented. The width and the height of the board were 23 mm and 52 mm, respectively, for mounting on the ID card.

The top requirement for the hardware design is energy efficiency, hence we seek to achieve one-year lifetime for a coin battery system. The proposed system contains only two sensors for localization: a magnetometer and an accelerometer. An accelerometer is essential for (i) the transformation from B_{raw} to B_{hv}, (ii) the PDR technique, and (iii) inferring the user's orientation. Other sensors, such as a gyroscope sensor and a barometer, can help enhance the localization performance; however, they were excluded from the present design, to reduce

Fig. 5. The implemented localization IoT device, in the form of an ID card on which a small board is mounted. The board contains a magnetometer, an accelerometer, and a BLE interface.

the device's energy consumption. We chose a KMX62-1031[16] sensor, which is an ASIC that consists of a 3-axis magnetometer and a 3-axis accelerometer.

For wireless communications, we chose a BLE chip [29] owing to its energy efficiency [28]. The BLE chipset used on the board was nRF52832 [21]. To localize the card's user in real time, the card/device continuously broadcasts a BLE advertisement frame that contains its sensor data. Thus, tuning advertisement-related parameters, such as the Tx interval and the Tx power, is a necessary step toward achieving energy efficiency. We set one second to be the Tx interval and -20 dBm to be the Tx power, to achieve the battery lifetime of one year, which was demonstrated in preliminary experiments. In the case of the Tx interval, one second is sufficient for tracking the position of the device's user. However, -20 dBm for the Tx power might be too weak for detecting at a certain distance, which required us to conduct the following experiments.

Table 1 shows the observation probability of the BLE beacon frames vs. the distance between the BLE access point (AP) and the Tx device, with the Tx power set to -20 dBm. The observation probability decreases for distances longer than 10 m. In our experimental environment, four BLE APs were deployed at every corner of a square-shaped office area in a grid format, and the length of a side of a square was 20 m. The case in which every AP received no beacon frames consecutively occurred infrequently during the entire evaluation process, owing to many APs. To make up for missing a single beacon frame, the device also sends the magnetic field data of the previous round.

4.2 Structure of the BLE Beacon Frame

Figure 6 shows the message format of the BLE advertisement frame, which is used for conveying the sensory data from an IoT device to a localization server in our system. The maximal size of the BLE advertisement frame is currently 31 bytes according to [29]. In the proposed system, the available space for the sensory data is 19 bytes, since 12 bytes are reserved for other data, including the company ID, the device's status, the remaining battery level, and the sequence number. We first contain a series of three pairs B_h and B_v in the current round (1 round = 1 s), where each value is 2 bytes long. Recall that the sensing rate is 3 Hz. Note that each value ranges from -1200 uT to +1200 uT [16]. Thus, the total number of bytes for reading magnetic vectors is 12. Then, the series of three $|B|$ values of the previous round needs 3 bytes; this is to make up for beacon missing cases, as mentioned in

Table 1. The observation probability of BLE beacons vs. distance, for the Tx power of -20 dBm.

Distance (m)	Observation Count	Transmission Count	Observation Probability
1	57	57	1.00
3	79	79	1.00
5	57	57	1.00
7	59	59	1.00
10	70	80	0.88
15	63	73	0.86

Item	*Metadata (seq. #, battery, status, ...)*	B_v	B_h	*last |B|*	*|acc|*	*Orientation*
Bytes	12	6 (3 * 2 bytes)	6 (3 * 2 bytes)	3 (3 * 1 bytes)	3 (6 * 0.5 bytes)	1

Fig. 6. A BLE beacon frame contains the magnetic data, accelerometer data, and orientation data.

Section 4.1. Even though a single value ($|B|$) may make it difficult to distinguish the magnetic fingerprint of one location from others, we cannot afford to keep two values (B_h and B_v) for the previous round, due to the space limit. In the case of the accelerometer, its sensing rate is 6 Hz, and each reading needs 0.5 bytes for its vector strength. Overall, that requires $6 * 0.5 = 3$. The acceleration data itself are used only in the step detection, and the detection algorithm does not require high-resolution data, as will be detailed in Section 5.3.1. The last byte is assigned to the average value of the orientation observed in the current round. The change of the user's heading direction in the indoor space tends to be not so frequent. Thus, a single orientation value per second is sufficient to track the direction of the user's movement.

4.3 Processing Sensor Data

In the proposed system, the device delivers the sensor readings to a back-end server via BLE APs. In this way, device-end data processing is minimized for energy saving purposes. However, owing to the space limitation of the BLE advertisement frame, front-end processing of sensory data should be performed in the device to compress the data that are to be delivered. Figure 7 shows the device architecture including data processing components and their inputs/outputs. Calculating $|acc|$, transforming a three-dimensional magnetic vector to a two-dimensional value (denoted by B_{hv}) [17], and averaging the orientation values [20] are straightforward.

As to extracting the gravity vector from the raw accelerator vector, many papers [11, 42, 44] have used an N-order Butterworth low pass filter (LPF) [5]. However, despite its good filtering performance, the Butterworth filter has $O(N \log N)$ time complexity [36] of the fast Fourier transform (FFT). Thus, it requires too much computational power and memory for IoT settings. We note that the main purpose of extracting the gravity vector is to obtain B_{hv} by rotating B_{raw} onto the gravity plane. For lightweight operations, we replaced the Butterworth filter by a first-order LPF as follows, since a simple LPF can calculate B_{hv} approximately.

$$y_i = a * x_i + (1 - a) * y_{i-1} \tag{1}$$

where x_i is an input value at the current time i, and y_i, y_{i-1} are output values at the current time i and previous time $i - 1$, respectively. Here, a is a constant for the LPF.

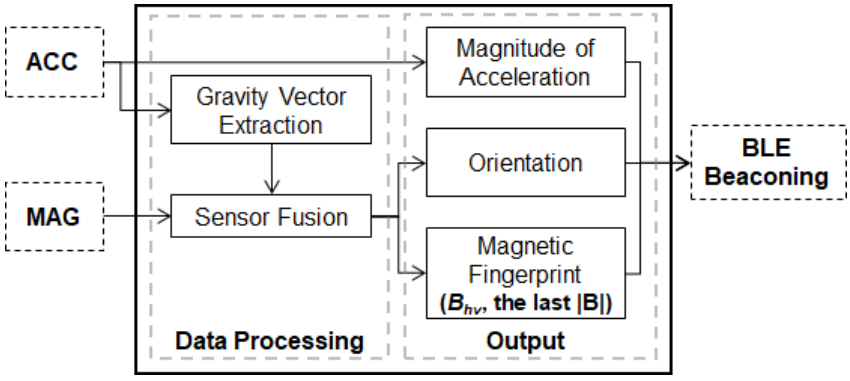

Fig. 7. The building blocks of the proposed indoor positioning device: a magnetometer, an accelerometer, and a BLE interface.

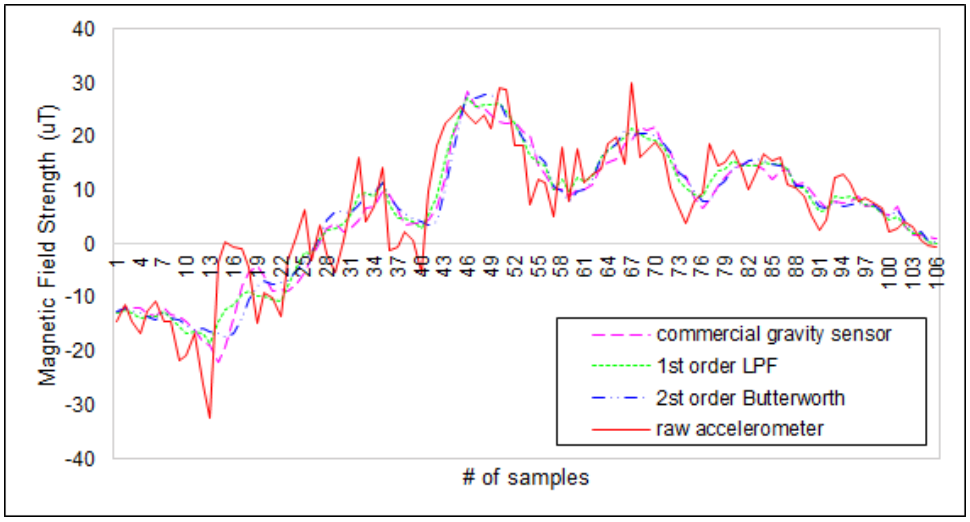

Fig. 8. Magnetic fingerprints extracted using different gravity vectors, for the same path.

Equation (1) is a simplified formula for the first-order LPF. This LPF is much simpler than the Butterworth filter and requires memory only for a single floating number y_{i-1}. To evaluate the performance of filters, we first recorded the acceleration data and B_{raw} while walking along the corridor, and rotated the B_{raw} vector by different gravity vectors extracted using different filters. A gravity vector obtained using a commercial gravity sensor of Samsung Galaxy S5 and a magnetic fingerprint rotated by raw acceleration were also used for comparison. Figure 8 plots only B_v, which shows that the patterns of magnetic fingerprints are almost similar. We thus used the simple first-order LPF in Equation (1).

As the final validation process, we compared the magnetic fingerprints obtained by a smartphone and the presently designed IoT device. The two fingerprints exhibited almost the same pattern along a 150-m-long trajectory in terms of B_h and B_v, respectively, as shown in Figure 9.

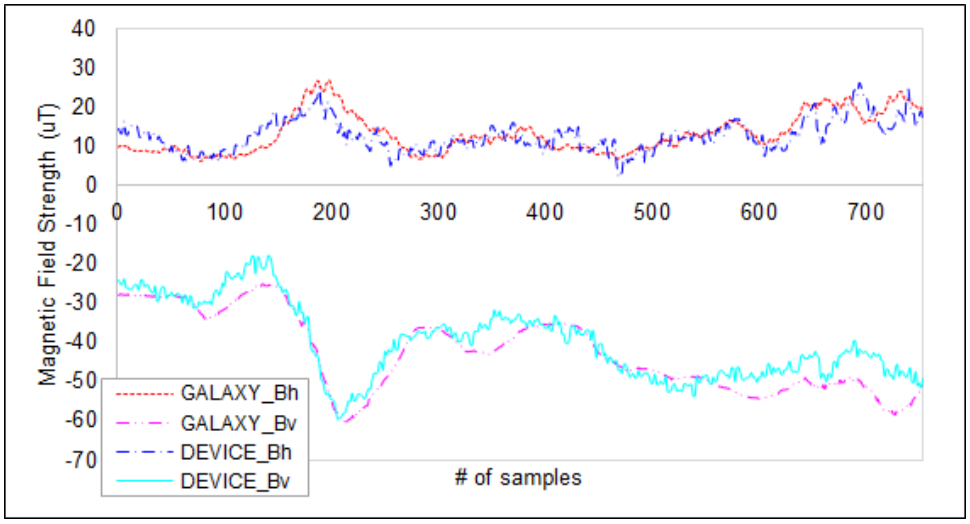

Fig. 9. Magnetic fingerprints obtained from a smartphone and the designed IoT device, for the same path.

5 SYSTEM ARCHITECTURE

We now introduce the architecture of the proposed system and the positioning algorithm, whose designs are based on the findings described in the previous sections.

5.1 Overview

In the proposed system, the positioning algorithm starts when a user carrying a neck ID card enters the target area. The card/device periodically advertises a BLE beacon frame with sensor readings as specified in Figure 6. The BLE APs positioned in a grid-like manner (intervals of 20 m) then receive the frame, which in turn is delivered to a back-end server. The APs each collect the received signal strength (RSS) of the received beacon frame for localization purposes. We analyze the BLE RSS along with the magnetic field data, to enhance the localization performance.

After receiving the beacon frames, the back-end server estimates the location of the user, using the particle filter algorithm. The computation is performed for each period (period duration, 1 s). The server first counts the number of footsteps and moves the particles depending on the step count and the orientation. Then, the user's final location is estimated using the particle filtering process, which will be described in details below.

5.2 Site Survey Methodology

For the site survey, we used the same magnetic fingerprint collection method as in Maloc [37]. In Maloc [37], the surveyor collected (and interpolated) magnetic fingerprints at every 0.1m * 0.1m grid points by moving in the target area along straight-line paths. However, storing fingerprints with such a fine granularity leads to a huge fingerprint database and high computational cost. What is worse, as the number of measurement points increases, there are likely to be more points with the same or similar magnetic reading. To determine the suitable size of a grid unit, we divided a 2-m-wide corridor into seven straight-line paths with 0.3 m intervals, which were numbered from 1 to 7, from the left to the right direction. Figure 10 shows the magnetic fingerprints along the different paths. We found that two adjacent fingerprints exhibited similar patterns, while next-nearest fingerprints tended to exhibit distinct patterns. Moreover, using the insights in 3.3, we also estimated the proper grid size by

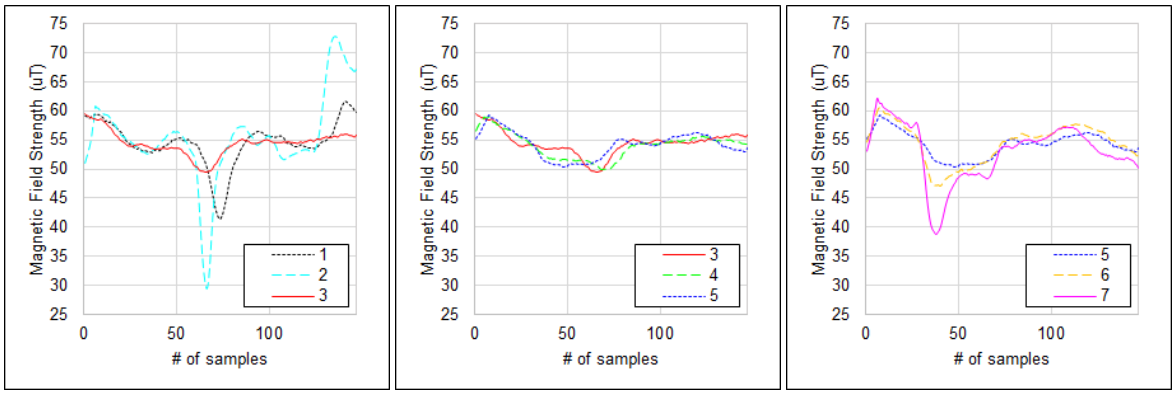

(a) Left-side paths (b) Middle paths (c) Right-side paths

Fig. 10. Fingerprints collected along multiple paths (in a corridor), with the distance of 0.3 m between adjacent collection sites.

observing the magnetic data along the same path. That is, the spatial change in the magnetic field data along a path was marginal for a certain distance. If the sensing rate of 3 Hz is sufficient for tracking the magnetic fingerprint pattern of a user when the user walks at a normal speed ranging from 1 m/s to 1.5 m/s, we can obtain only one or two fingerprint data for each 0.5 m unit as a representative value. We thus chose 0.5 m as the grid size based on the above findings.

We implemented an Android application for convenient site surveying, and Figure 11 shows a screenshot of this application. The surveyor can easily choose the target grid for measurements. We also incorporated a PDR module into the application, hence allowing to map collected fingerprints to proper grids, even if the surveyor walks at various speeds. Note that we use the average values of B_h, B_v, and the RSSs received by the BLE APs nearby as the fingerprint of each grid.

5.3 Particle Filter Framework

In this section, we explain the particle filter framework that is used in the proposed system. The particle filter solves the filtering problem, which amounts to estimating the state of a dynamical system (i.e., the location of a user) from noisy and partial observations. The key action of the particle filter consists of distributing a set of particles (also called samples) in each epoch, to represent the probability distribution of the state of the dynamical system. In the next epoch, the observation is different, owing to the dynamical nature of the system, which is manifested as replacement of old particles (of negligible probabilities) by new particles or moving particles into a new distribution.

5.3.1 Step Counting. First, we should count the number of steps for moving the particles. In our system, there are only six $|acc|$ values per second owing to the space limitation on the beacon frame; thus, we use a simplified heuristic algorithm for counting the number of steps. We adopted the peak-valley detection technique [7, 18, 24], which allows to count the steps using a simple algorithm. It is widely known that the temporal change in the acceleration (of a walking user) exhibits a periodic pattern of alternating peaks and valleys. Thus, steps can be counted by tracing this pattern.

We collect the acceleration magnitude (i.e., raw floating data) as the user walks 15 steps with the sampling frequency of 15 Hz, as shown in Figure 12(a), and the measurements are filtered by the proposed system (6 Hz,

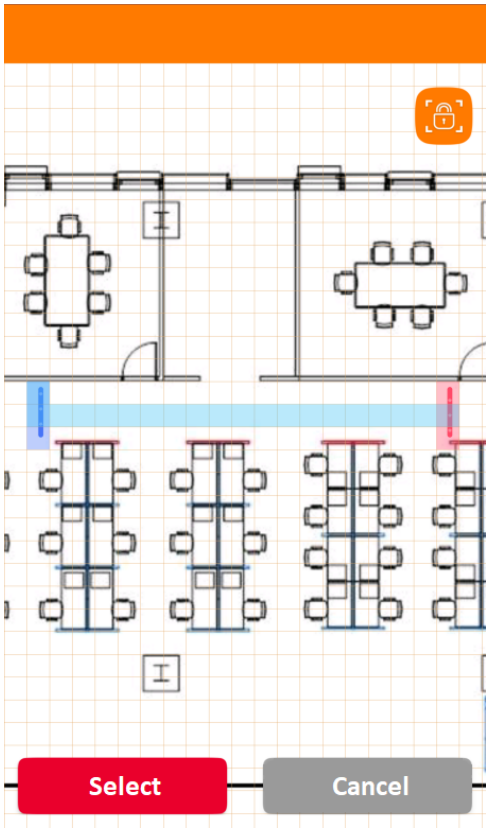

Fig. 11. A screenshot of the site survey app, captured to illustrate the convenience of fingerprint measurements.

rounded off to integers), as shown in Figure 12(b). To clearly trace the peaks and valleys in our measurements, we designed the device firmware to compute the maxima and minima of the acceleration magnitude three times during a time window (1-s-long window). Thus, three max-min pairs (of the acceleration magnitude data) for each time window are transmitted over the BLE interface. Obviously, some information is lost owing to compression, but the data critical for the peak-valley detection technique are delivered. Next, we determine the peaks and valleys in the sequence by applying two thresholds: $12m/s^2$ for the peaks and $8m/s^2$ for the valleys. We also consider the increasing and decreasing trends in the overall sequence for excluding false peaks and valleys. The red dots in Figure 12(b) show the results obtained using our step-counting algorithm. The accuracy of the step-counting algorithm over the entire evaluation process was above 90%.

5.3.2 Motion Model. Although the distortion in the magnetic field in an indoor environment can be used as a fingerprint, it also hinders us from inferring the heading orientation of a user/device. This phenomenon directly and negatively affects the performance of the particle filter technique, because particles should move in the same direction as the user's orientation. To overcome this problem, we adopted a technique that was introduced in Magicol [26]. Magicol exploits the observation that a walking human is very likely to follow the direction of a corridor, rather than making random turns. However, we have to propose an alternative solution because we cannot use a gyroscope sensor (to track the user's heading more correctly) as in Magicol.

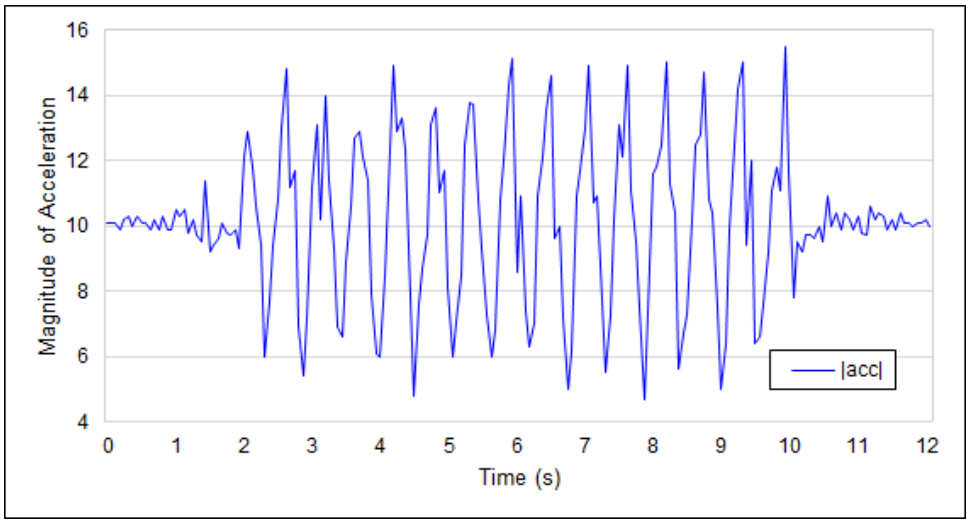

(a) raw acceleration data (15Hz)

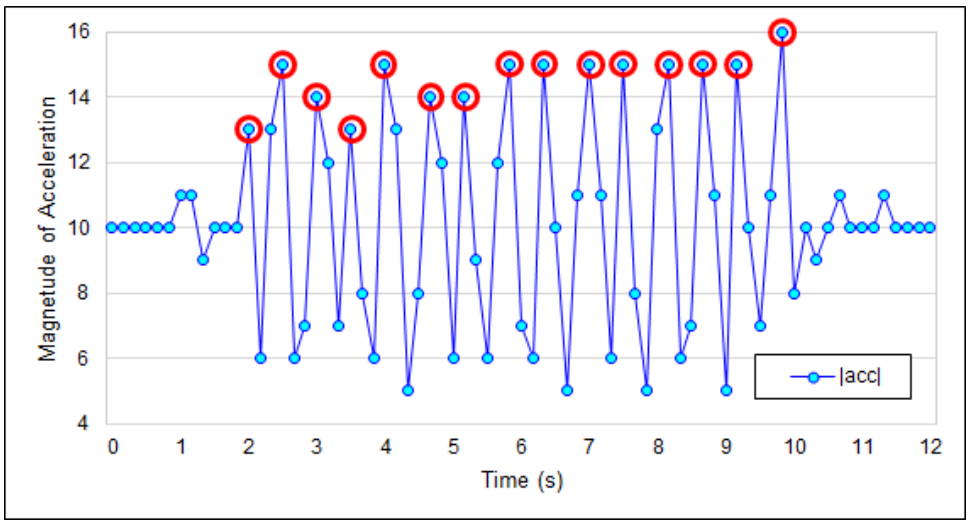

(b) acceleration data from our device (6Hz) and step counting result

Fig. 12. The temporal pattern of the acceleration magnitude and the result obtained using the proposed step-counting algorithm, for a user walking 15 steps.

To ensure that particles follow the user's walking direction, we take a probabilistic approach substantiated in Algorithm 1. Forty percent of the particles move along the pathway (one out of several candidate pathways) whose direction is closest to the orientation reading of the device. Another 40% of the particles choose a direction by considering the extrapolation of the user's movement between the previous and current rounds. The remaining 20% of the particles move simply following the raw orientation reading (regardless of the pathway). The proposed

Algorithm 1: The algorithm for the estimation of heading in the particle filter framework.

Input: θ_{raw} = Raw orientation from sensor reading
Input: θ_p^{t-1} = Orientation in the previous round of each particle p
for *each particle p* **do**
  $prob$ = choose a random number between 0 - 1.0;
  if $prob < 0.4$ **then**
    θ_{path} = choose the closest orientation to θ_{raw} from the directions of the pathway where p is on;
    if $|\theta_{path} - \theta_{raw}| < 90$ **then**
      move p towards θ_{path};
    else
      move p towards θ_{raw};
    end
  else if $0.4 <= prob < 0.8$ **then**
    θ_{path} = choose the closest orientation to θ_p^{t-1} from the directions of the pathway where p is on;
    if $|\theta_{path} - \theta_p^{t-1}| < 90$ **then**
      move p towards θ_{path};
    else
      move p towards θ_{raw};
    end
  else
    move p towards θ_{raw};
  end
end

model is thus likely to force most of the particles (~80%) move along the (estimated) pathway direction. Figure 13 shows that this algorithm (indicated by Motion Model) traces the user's walking orientation with the accuracy of 84%, even if the user makes 11 turns on the trajectory. Here, GT denotes the ground truth direction of the user. Note that the magnetic reading for the orientation can be far from the real direction of the user, owing to distortion.

While other magnetic field-based systems, such as Maloc [37] and Magicol [26], aggressively leverage the accurate estimation of orientation using a gyroscope, the proposed motion model achieves high accuracy in spite of the much lower sensor rate (1 Hz) and the absence of a gyroscope. Our probabilistic approach that tracks both the pathway's direction and the history of the user's trace effectively estimates the user's true orientation in structured indoor environments. The performance of the motion model directly affects the posterior distribution of states in the particle filtering framework.

5.3.3 Magnetic Matching. After all particles move, the survival probabilities (weights) of the particles need to be computed. As described in 3.1, the weight of a particle is computed using the temporal history of B_{hv} as a fingerprint to overcome the low distinctiveness of magnetic field data. Prior approaches [26, 32] that used magnetic field history data exploited the DTW algorithm to compare the similarity between magnetic fingerprints to support various walking speeds. However, the DTW technique is expensive both computationally and memory-wise, especially when used with the particle filter framework that computes the weight of every particle. Thus, in our approach we exploit the Euclidean distance to lower the computational complexity when comparing the similarity between the observed fingerprint and patterns in the database.

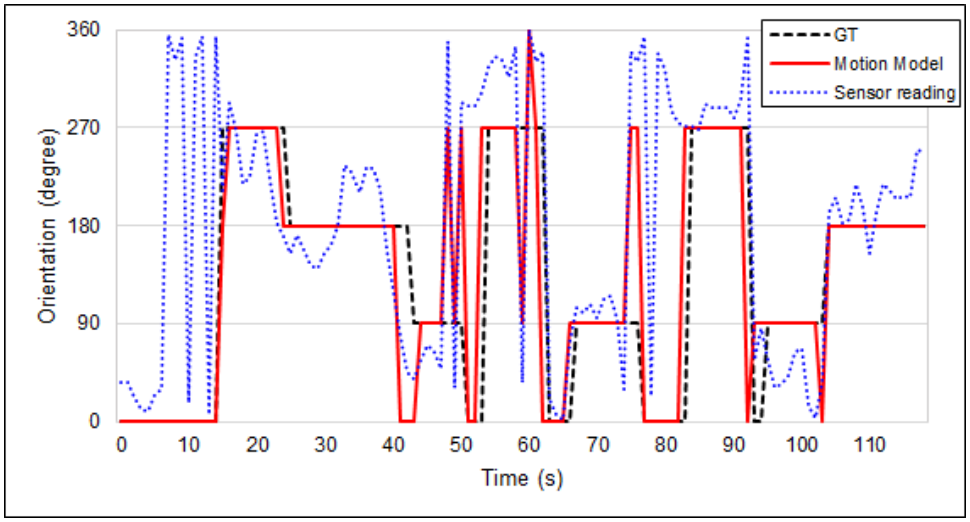

Fig. 13. Performance of the motion model algorithm for inferencing the user's orientation. Raw orientation readings were obtained and calibrated by the motion model that achieved 84% accuracy on a trajectory with 11 turns.

To exploit the Euclidean distance to find the matching entry in the database, the speed of the user's fingerprint measurements should be estimated first. As explained in Section 3, various walking speeds and sensing rates of the device along the same path may generate seemingly different fingerprint patterns. As the sensing rate is fixed at 3 Hz in the proposed system, the issue that remains to be resolved pertains to different walking speeds of the user and the (site) surveyor. We resolve this issue by (1) allocating a wide range of stride lengths for each particle, and (2) disseminating the particles in a wider area in the proposed particle filter framework during the resampling of dead particles. With the sensing rate fixed, the differences between the fingerprint patterns of different users are relatively small. Thus, moving the particles to some area including the true location of the user is easily achieved using the two above-mentioned techniques. Although we should use many particles (about 3000) to cover the wide range of stride lengths and hence the wide area of dissemination during the resampling, the increase in the execution time with the Euclidean distance is much smaller than the one for the DTW technique (detailed in Section 6).

5.3.4 BLE Matching. In our approach, we also used the BLE matching technique as a supplement to the particle filter framework. We first adopted a traditional fingerprinting approach introduced in RADAR [2] for BLE matching. In the fingerprint database, each grid of the target area contains a BLE RSS fingerprint obtained during the site survey, which allowed us to infer the best-matched grid by comparing the user's BLE RSS observation and the database content. However, owing to the weak strength of BLE signals compared with WiFi, the localization performance of BLE fingerprinting may be somewhat unstable. Thus, augmenting the BLE matching results with particle weighting does not improve the overall performance of the system.

When we extend the magnetic field data in the time domain for fingerprinting, we should decide how many readings of the magnetic field data will be sufficient for achieving the desired localization performance. To this end, we conducted a pilot experiment to decide the time duration that is necessary to make the temporal history of magnetic readings distinct; it took about 10 s (10 m to 15 m in the moving distance) for a sequence of magnetic data to have distinctiveness. Hence, we used the BLE matching combined with the magnetic fingerprint to improve the overall localization performance. For the first 10 s after the initialization, we remove the particles

that are beyond a certain range R_{BLE} from the BLE matched grid. Note that the particles around the GT point should not be removed. For that, we count how many times a particle is outside the R_{BLE} range consecutively; if the particle is outside for τ_c times, it is removed. We call this technique *BLE filtering*. Also, we set τ_c to 2 and R_{BLE} to 6 m to speed up the convergence of the particle distribution.

5.3.5 Particle Filter. We now combine the above component processes into a particle filter framework. Equation 2 shows the particle model for particle p_i in the proposed system

$$p_i =< x_i, y_i, \theta_i^{t-1}, w_i, c_i, \vec{h} > \tag{2}$$

where x_i, y_i represent the current location of particle p_i, which captures the candidate user location. θ_i^{t-1} is the orientation measure in the previous round (i.e., $t-1$) and w_i represents the weight of the particle. c_i and $\vec{h}$ denote the *BLE filtering* count of the particle and the temporal history of B_{hv} that the particle has observed along its trajectory, respectively.

During the initialization phase, the particles are uniformly distributed throughout the target area. Then, for each beacon, the position and the weight are updated. At first, the position of particle p_i at time t is updated based on the step-counting and motion model algorithms, using Equation 3

$$(x_i^t, y_i^t) = \begin{cases} x_i^t = x_i^{t-1} + N_{step}^t \times (l + G_l) \times \cos(\theta_{mm}^t + G_\theta) \\ y_i^t = y_i^{t-1} + N_{step}^t \times (l + G_l) \times \sin(\theta_{mm}^t + G_\theta) \end{cases} \tag{3}$$

where N_{step}^t is a detected step count at time t, l is 0.65 m as a mean value of the stride length distribution, and θ_{mm}^t represents the calibrated orientation obtained using the motion model. G_l and G_θ are Gaussian noise processes of the stride length and orientation, respectively.

We add a relatively higher Gaussian noise to the stride length as $G_l \sim \mathcal{N}(0,\ 0.5l)$ compared with the existing approaches (e.g., $\sigma = 0.2l$ as used in [26]), to expand the distribution area of the particles to support various walking speeds (of users). The Gaussian noise for the orientation is set to $G_\theta \sim \mathcal{N}(0,\ 10^\circ)$.

After the particles move, their weights should be updated. In our approach, we adopted a Gaussian weight function, following [26]. The Gaussian function effectively enhances the distinctiveness of the magnetic fingerprint patterns owing to its bell-like shape. Equation 4 describes the weight function

$$w_i = \alpha e^{-\frac{\|d\|^2}{2\sigma^2}} \tag{4}$$

where α is the height of the Gaussian curve's peak and the maximal value of the magnetic weight, σ is the aggressive parameter to control the width of the Gaussian curve, which captures how aggressively the weight decreases as $\|d\|$ increases. Here, $\|d\|$ is the Euclidean distance, as shown in Equation 5

$$\|d\| = d(\vec{h}, \vec{u}) \tag{5}$$

where $\vec{u}$ is the vector of B_{hv} measured by the device.

Note that the mean removal technique is applied to $\vec{h}$ and $\vec{u}$, respectively, as explained in Section 3.2. After updating the particle's weight, the particle is removed if it satisfies any of the following conditions.

(1) The particle hits the wall
(2) w_i is lower than a threshold τ_w
(3) BLE filtering

The final phase of the particle filter algorithm is resampling and the inference of the user's location. As explained in 5.3.3, we adopt here a heuristic algorithm to maintain a sizable area for particle dissemination to support various walking speeds of users. For the removed particles, we replenish the same number of new particles around the survived particles with top 10% of weights. At this moment, the distance between surviving

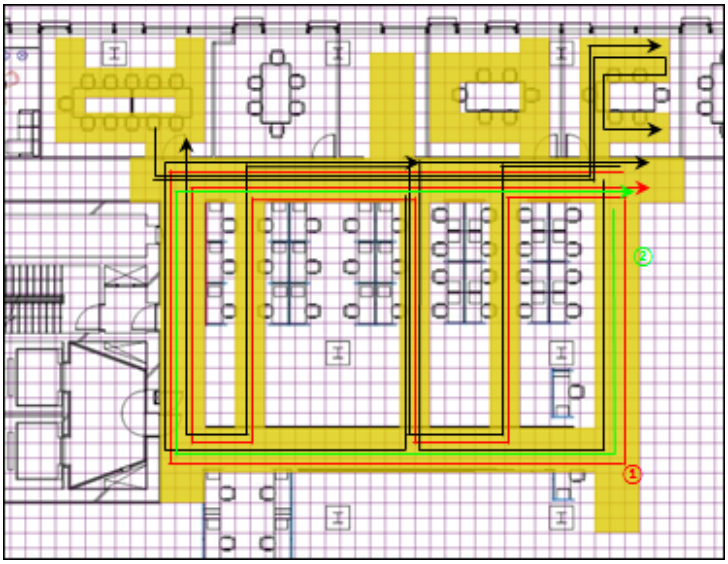

Fig. 14. Evaluation of the proposed system in a 20.5 m × 16 m office area with three conference rooms.

and replenished particles is randomly distributed within a circular area of its radius being 1.5 m. Finally, to infer the final location of the user, we calculate the average of the coordinates over all of the particles, weighted by w_i.

6 EVALUATION

In this section, we evaluate the proposed system in terms of the localization accuracy, computational cost, as well as energy efficiency. The evaluation consists of (1) parameter tuning for the particle filter algorithm such as the temporal sequence of $\vec{h}$ and number of particles P, (2) comparing the effectiveness of the Euclidean distance (EUC) approach with the DTW approach, and (3) measurements of battery consumption for the prototype device.

6.1 Implementation

We first implemented an IoT device for localization, as shown in Figure 5, and its firmware as described in Section 4. When the testers carrying the device walked in the target area, the device continuously delivered sensor readings to the back-end server via the BLE APs. Note that the four BLE APs were organized in a grid-like manner (with 20 m intervals) at the four corners of the testbed. Then, the particle filter framework implemented on the back-end server PC with a 3.3 GHz CPU and 16 GB memory estimated the location of the device based on the sensor readings. The particle filter framework could perform both real-time and off-line analysis after collecting user traces. We chose the latter to evaluate the proposed system against the ground truth for the sake of simplicity.

6.2 Experiment Setup

To evaluate the performance of the proposed system in a real-world setting, we collected sensory data in a 20.5 m × 16 m office area, as shown in Figure 14. The target area contained three conference rooms and multiple corridors. To support the various moving speeds and stride lengths of target users, three testers with different heights collected the data for three months, from February to April of 2017. We defined seven trajectories in the target area, among which two trajectories each were tested at three speeds (0.58 m/s, 0.91 m/s, and 1.30 m/s) and

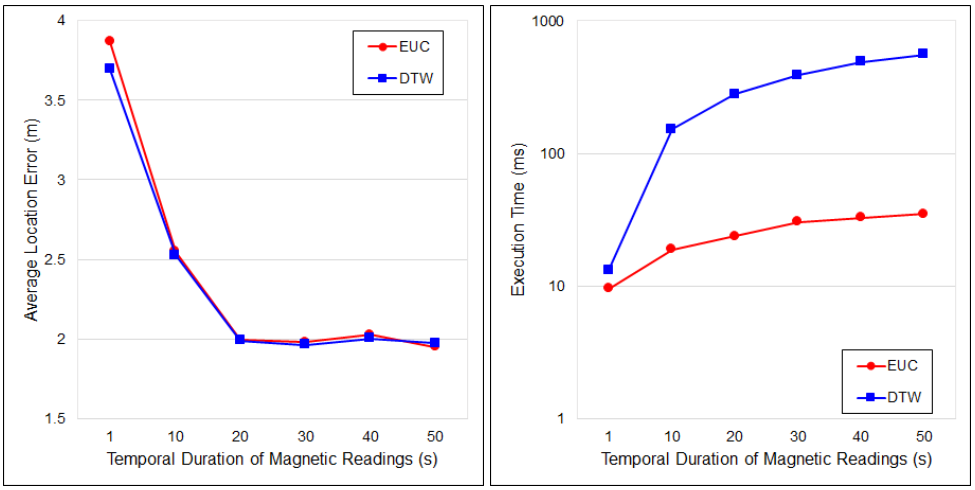

(a) Localization performance (b) Execution time

Fig. 15. Effect of the temporal duration of magnetic readings on the localization performance and on the execution time.

three device heights (0.9 m, 1.1 m, and 1.3 m). The other five trajectories were tested for speeds in the 1.0 - 1.1 m/s range. In Figure 14, two trajectories are drawn in red and light green, and the others are drawn in black. Using the collected data, we evaluated the system in terms of the localization accuracy, computational cost, and energy efficiency.

6.3 Localization Performance

6.3.1 Temporal Duration of Magnetic Readings. We first evaluated how the temporal duration of the magnetic readings (i.e., $\vec{h}$) affected the localization performance in Figure 15. Figure 15(a) compares the localization accuracy of the Euclidean distance (EUC) and the DTW algorithms, for different temporal duration of $\vec{h}$. Note that we assigned 3000 particles in this experiment. Figure 15(a) shows that both algorithms achieved the accuracy of 2 m when we set the temporal duration of $\vec{h}$ to be longer than 20 s. The execution times for the EUC and DTW methods, plotted in Figure 15(b), show that the difference between the EUC and DTW methods increases significantly with increasing temporal duration of $\vec{h}$. Interestingly, the execution time of the EUC algorithm appears to converge, even when the temporal duration of $\vec{h}$ increases. Hence, we conservatively chose 30 s as the temporal duration of magnetic readings (i.e., 90 samples) in what follows.

6.3.2 Number of Particles. The number of particles, P, in the particle filter algorithm is a key parameter directly linked to the localization performance and the computational cost. Figure 16 shows the time-series localization performance when a target user walks along the trajectory ① as shown in Figure 14. We assigned two numbers to P: 500 (Figure 16(a)) and 3000 (Figure 16(b)).

With $P = 500$, as shown in Figure 16(a), the EUC method poorly traces the movement of the target user when two turns are made with a short interval (around 75 and 79 s). It then spends almost 30 s on catching up with the target user at the similar localization accuracy as the DTW method. The main reason for the poor performance of the EUC method with $P = 500$ is that a wide but sparse distribution of particles may not cover the ground-truth location of a target user. On the other hand, in the case of $P = 3000$, as shown in Figure 16(b),

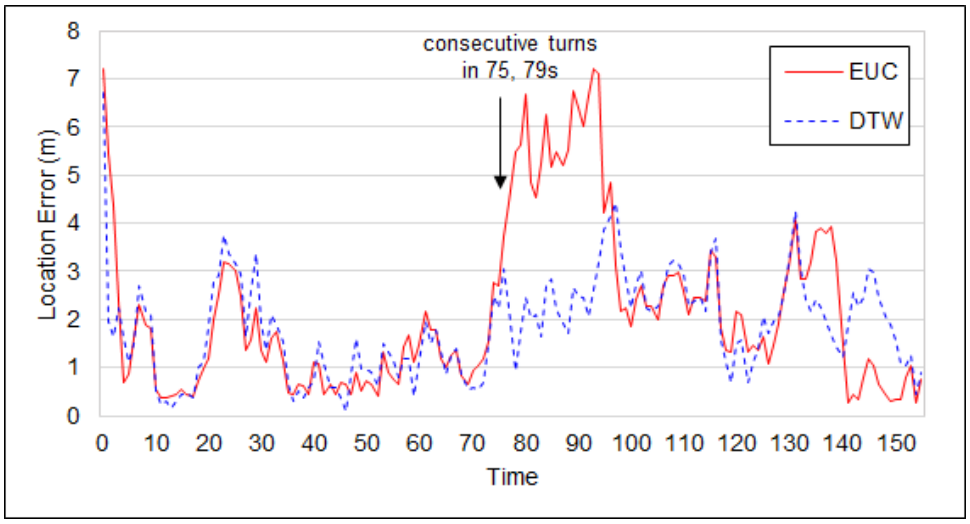

(a) $P = 500$

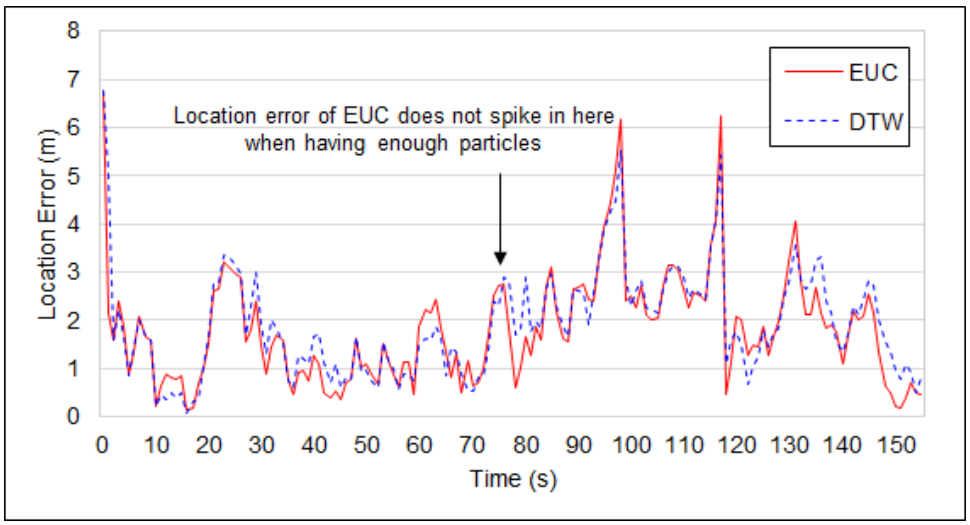

(b) $P = 3000$

Fig. 16. Localization performance of the EUC and DTW methods, for different numbers of particles in a long trajectory.

the localization errors for the EUC method around 75 s and 79 s do not spike owing to the sufficient density of particles. Interestingly, the EUC method with $P = 3000$ performs even better than the DTW method with the same number of particles. That is, the average localization error of the DTW method is 1.92 m, while that of the EUC method is 1.81 m. All of the experiments for all scenarios demonstrated the same tendency, as shown in Figure 19(a). As shown in Figure 19(a), using the DTW method with $P = 500$ ($DTW500$) was slightly advantageous

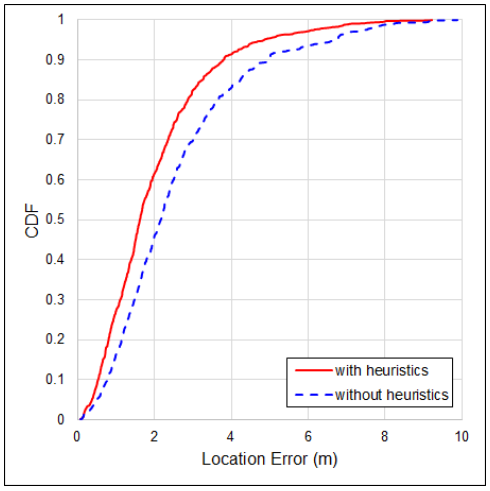

Fig. 17. Effect of the heuristic algorithms in Section 5.3.5 for a system with 3000 particles in the particle filter framework.

to using the EUC method with $P = 500$ ($EUC500$), but the performance gap between the $DTW3000$ and $EUC3000$ methods was negligible, owing to the sufficient number of particles.

We also evaluated the effect of the heuristic algorithms (in Section 5.3.5) that can contain the candidate locations (by placing the particles as explained in Section 5.3.5) when they run with the sufficient number of particles, $P = 3000$. Figure 17 compares the results for $EUC3000$, with and without these heuristic algorithms. As shown in Figure 17, the performance of the EUC method without these heuristic algorithms is significantly compromised, which implies that these heuristic algorithms are effective when a sufficient number of particles is used.

We next compared the computational cost of the EUC and DTW methods, and the results are shown in Figure 18. Figure 18 shows the computation time for a single-round particle filter algorithm. As shown in Figure 18, the EUC method is more computationally efficient. Since we set the temporal duration of $\vec{h}$ to 30 s, the accumulated history size of the DTW method gradually increases until 30 s from the start, and maintains the same size after that point. On the other hand, the execution time of the EUC method is almost the same up to 30 s from the start. Moreover, the EUC method yields a 15x faster execution time than the DTW method on average (450 ms for DTW, 30 ms for EUC). This also holds for different scenarios with different P, as shown in Figure 19(b). Note that the execution time of $DTW500$ is even 2.7x times longer than that of $EUC3000$; the median execution time of $EUC3000$ is 29 ms, while that of $DTW500$ is 78 ms. Considering the comparable localization performance of $EUC3000$ and $DTW3000$, as shown in Figure 19(a), we conclude that leveraging the Euclidean distance can achieve a comparable localization performance to that of the DTW approach, while being more computationally efficient (and thus more energy efficient).

Finally, we set the number of particles to 3000 in the proposed system, i.e., $EUC3000$. Figure 19(a) shows the localization errors for the different algorithms. For comparison, we also evaluated the PDR-based particle filter algorithm (PDR_RAW) without the motion model and the BLE fingerprinting algorithm adopting RADAR [2] (BLE_RADAR). The average localization error of the proposed system for every scenario was 1.96 m, and the median error was 1.62 m. This result indicates that the proposed system performs almost as well as systems that use smartphones [26, 37] and the DTW approach. At the same time, the proposed system is more computationally efficient than other systems, as shown in Figure 19(b). In comparison with Magicol [26] and Maloc [37] approaches, for which the execution times are longer than 3 s and 1 s, respectively, our system performs much faster owing

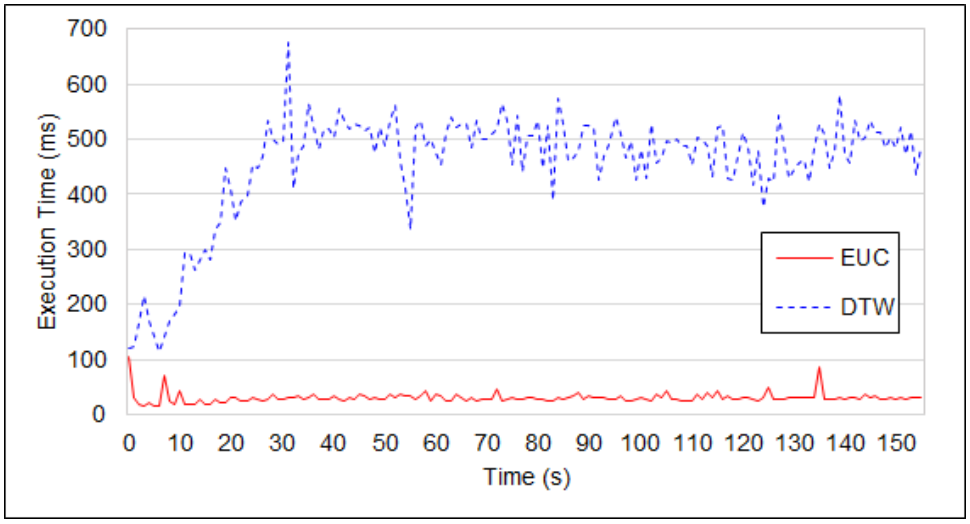

Fig. 18. Comparison of execution times of the EUC and DTW methods, with $P = 3000$, for a long trajectory.

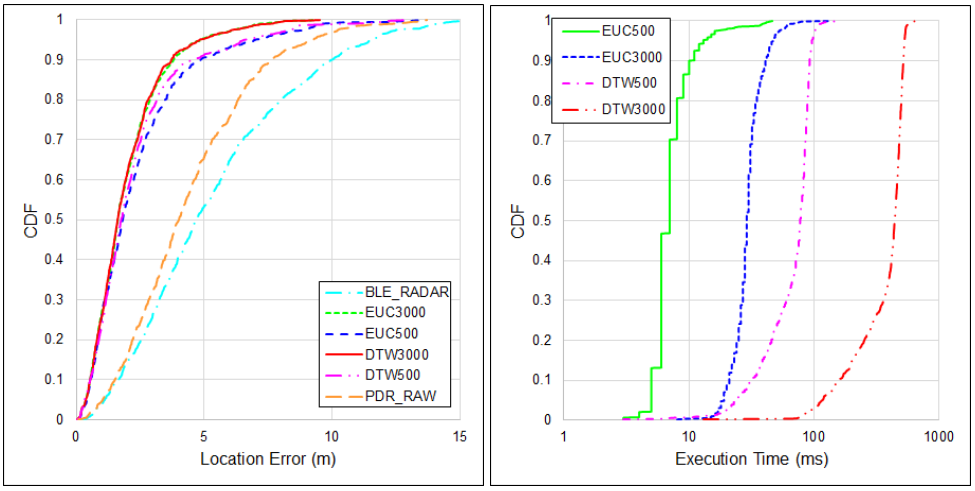

(a) Localization performance (b) Execution time

Fig. 19. Localization performance and execution time for different algorithms, for different numbers of particles P.

to the smaller number of sensors and data rate, and because it does not use computationally heavy algorithms such as the DTW algorithm.

6.3.3 BLE Filtering. Figure 20 analyzes the efficiency associated with incorporating the *BLE filtering* technique into the particle filter framework. As shown in Figure 20(a), *BLE filtering* reduces the localization error and its convergence time, especially in the first part of the experiment. Figure 20(b) shows the cumulative distribution functions (CDFs) of the localization errors, for different scenarios. As shown in Figure 20(b), the localization

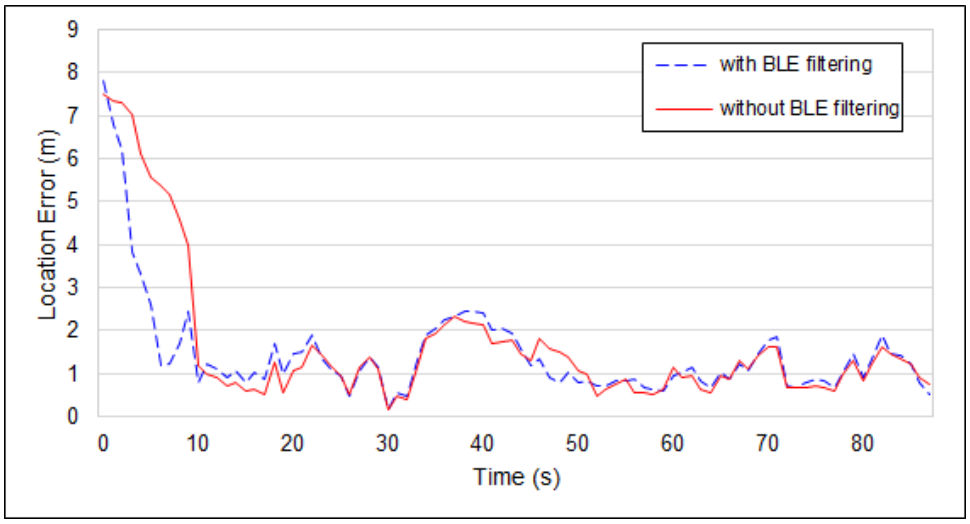

(a) The change in the localization performance as the user walks for 90 s

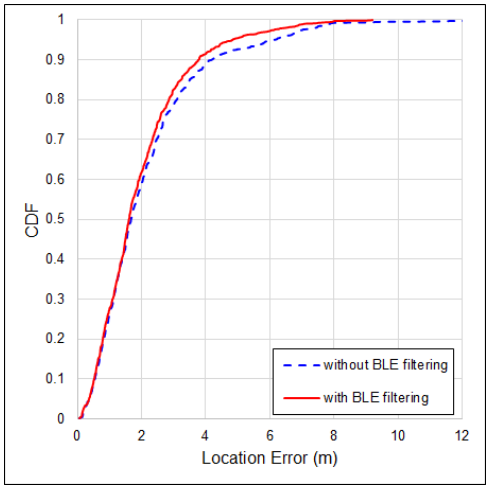

(b) CDFs of localization errors for all the experiments

Fig. 20. Effect of the BLE filtering technique.

performance is improved, especially for the cases with large localization errors, because *BLE filtering* reduces the convergence time.

6.4 Energy and Algorithmic Efficiency

We next evaluated the energy efficiency of the IoT device by measuring its energy consumption as shown in Figure 21. We observed that the device uses 0.159 mA in the active mode, during which it performs continuous BLE advertisements at 1 Hz, while it requires 0.004 mA in the sleep mode. The battery we used in the proposed

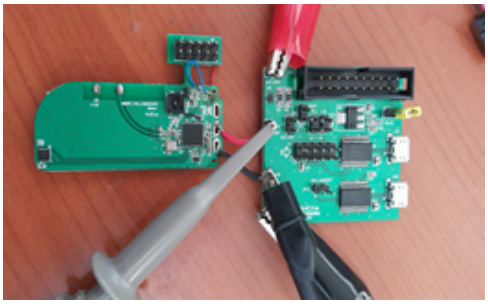

Fig. 21. We measured the energy consumption of the developed IoT device.

Table 2. The CPU usage of a typical back-end server vs. the number of devices.

Number of Devices	CPU Usage (%)
1	5.27
10	8.52
20	19.50
30	59.50
40	71.78
50	70.82
60	87.53

device was a CR2450 [9] with the 620 mAh capacity. Hence, assuming the device is used 8 h a day, the device can be used for 324 days. Note that switching between the active and sleep modes can be easily triggered by sensing the magnitude of acceleration.

We also evaluated how many IoT devices a typical back-end server (i.e., with 2.2 GHz CPU and 16 GB memory) can handle. To this end, we implemented a benchmark software that emulated multiple devices in the proposed particle filter system. As shown in Table 2, the CPU usage (of the back-end server) increased with increasing the number of devices. We found that a desktop-level machine can handle about 60 devices. Therefore, we expect that the proposed system can simultaneously support hundreds of devices with a high-end server machine.

7 DISCUSSION

Comparison with Other Indoor Localization Systems. We compared our system with other representative indoor localization systems in Table 3. Methods that leverage WiFi signals, such as Horus [39], are the most widely used ones, owing to the wide deployment of WiFi APs. However, WiFi scanning takes 3-4 s, and also consumes much energy. UWB-based systems [13] achieve very high accuracy on the centimeter scale and provide real-time positioning services. However, they still suffer from the problems of high energy consumption [23] and high deployment cost, due to the need for customized hardware devices. From the viewpoints of both energy consumption and scanning frequency, systems that are based on BLE [46] can be a good alternative. However, they are characterized by a high cost for dense installation of BLE beacons. Moreover, frequent fluctuations of these wireless signals (including WiFi, BLE, UWB), caused by the multi-path effect and human body blockage, often make the localization performance of these systems unstable. As a way to overcome the inherent weaknesses

Table 3. Comprehensive comparison with other representative indoor localization systems.

System	Technology	Accuracy	Algorithm Complexity	Cost	Energy Efficiency	Robustness
[39]	WiFi	2 m	Medium	Low	Poor	Moderate
[13]	UWB	39 cm	Low	High	Poor	Moderate
[46]	BLE	1.4-1.7 m	Low	High	Good	Moderate
[45]	Vision light	18 cm	Medium	Low	Poor	Poor
[37]	Magnetic	1-2.8 m	Medium	Low	Moderate	Good
[26]	Magnetic	1-2 m	High	Low	Moderate	Good
Our System	Magnetic	1.6 m	Low	Low	Good	Good

of wireless signals, some studies [41, 45] have proposed visible light-based localization systems. These systems achieve very high positioning accuracy and their deployment cost is much lower, because there are already ubiquitously deployed fluorescent lights and light-emitting diodes (LEDs) in buildings. The drawbacks are (i) high energy consumption associated with the camera operation and vision data analysis, and (ii) line-of-sight (LoS) path requirements on the light sources.

On the other hand, as explained in Section 3.1, the robustness and pervasiveness of magnetic fields make magnetic field-based systems more viable than systems based on other localization sources. The magnetic field is not affected by obstacles and is nearly stable in time, and its discernibility can be enhanced by using the temporal history of B_{hv} as a fingerprint. Compared with previous studies [26, 37], our system is more energy and algorithmically efficient. Our prototype IoT device achieves one-year battery life for a coin battery, by streamlining the amount of sensor data to process, and by simplifying the sensory data-processing algorithms. We suggest an augmented particle filter framework by introducing a robust motion model that achieves similar accuracy despite much smaller amounts of sensor data. The evaluation results confirmed that our system exhibits a similar level of positioning accuracy as previous magnetic field-based systems, while it is more computationally and energy efficient. Although the positioning accuracy of the system is slightly lower than those of UWB- and vision light-based systems, the median accuracy of 1.6 m is sufficient for most LBS-like tasks of tracking humans in workplaces, child care services, and emergency escape services.

Bluetooth 5.0. We used a BLE chipset based on the Bluetooth 4.2 specification in the proposed system, because the Bluetooth 5.0 specification was published after its hardware implementation. Adopting Bluetooth 5.0 [30] in the proposed system would provide a larger beacon frame length, up to 255 bytes. Without the space constraints on the BLE payload size, each device would be able to deliver more information to the back-end server, which is expected to enhance the performance. In this paper, we used a highly simplified version of PDR based on a low sensor rate (6 Hz for the accelerometer, 1 Hz for orientation), owing to the limitation of the payload size. Using a more sophisticated PDR technique (say [25]) with higher sensing rates of the accelerometer and the orientation sensor will likely improve the performance of the motion model and hence the performance of the entire system.

Deployment on Smartphone. The proposed system is equipped with the same type of sensors as the ones that are used in commercial smartphones. Thus, the proposed solution can be easily deployed in smartphones while reducing the computational cost and enhancing the system's energy efficiency.

8 CONCLUSION

In this paper, we designed and implemented a practical indoor localization system based on the magnetic field, for use in IoT applications. We first addressed the issues related to using the magnetic field for localization, and designed an IoT device equipped with a magnetic sensor, an accelerometer, and a BLE interface. Using the results of our preliminary experiments, we sought to streamline the computational overhead and the sensory data for localization. We also enhanced the efficiency of the particle filter algorithm by adopting multiple techniques. The comprehensive experiments reveal that the proposed system achieves the median localization accuracy of 1 m, while satisfying the low computational overhead and high energy efficiency requirements.

ACKNOWLEDGMENTS

This work was supported in part by the Ministry of Education of the Republic of Korea and the National Research Foundation of Korea (NRF-2017S1A5B8058870). Both the snu-samsung smart campus research center and the ICT at Seoul National University provides in part research facilities for this study.

REFERENCES

[1] Michael Angermann, Martin Frassl, Marek Doniec, Brian J Julian, and Patrick Robertson. 2012. Characterization of the indoor magnetic field for applications in localization and mapping. In *Indoor Positioning and Indoor Navigation (IPIN), 2012 International Conference on*. IEEE, 1–9.

[2] Paramvir Bahl and Venkata N Padmanabhan. 2000. RADAR: An in-building RF-based user location and tracking system. In *INFOCOM 2000. Nineteenth Annual Joint Conference of the IEEE Computer and Communications Societies. Proceedings.*, Vol. 2. IEEE, 775–784.

[3] Stephane Beauregard and Harald Haas. 2006. Pedestrian dead reckoning: A basis for personal positioning. In *Proceedings of the 3rd Workshop on Positioning, Navigation and Communication*. 27–35.

[4] Donald J Berndt and James Clifford. 1994. Using dynamic time warping to find patterns in time series. In *KDD workshop*, Vol. 10. Seattle, WA, 359–370.

[5] Stephen Butterworth. 1930. On the theory of filter amplifiers. *Wireless Engineer* 7, 6 (1930), 536–541.

[6] Krishna Chintalapudi, Anand Padmanabha Iyer, and Venkata N Padmanabhan. 2010. Indoor localization without the pain. In *Proceedings of the sixteenth annual international conference on Mobile computing and networking*. ACM, 173–184.

[7] John Chon and Hojung Cha. 2011. Lifemap: A smartphone-based context provider for location-based services. *IEEE Pervasive Computing* 10, 2 (2011), 58–67.

[8] Jaewoo Chung, Matt Donahoe, Chris Schmandt, Ig-Jae Kim, Pedram Razavai, and Micaela Wiseman. 2011. Indoor location sensing using geo-magnetism. In *Proceedings of the 9th international conference on Mobile systems, applications, and services*. ACM, 141–154.

[9] Energizer. 2017. Energizer CR2450 Specification. http://data.energizer.com/pdfs/cr2450.pdf. (2017).

[10] Andreas Ettlinger and Günther Retscher. 2016. Positioning using ambient magnetic fields in combination with Wi-Fi and RFID. In *Indoor Positioning and Indoor Navigation (IPIN), 2016 International Conference on*. IEEE, 1–8.

[11] Dominik Gusenbauer, Carsten Isert, and Jens Krösche. 2010. Self-contained indoor positioning on off-the-shelf mobile devices. In *Indoor positioning and indoor navigation (IPIN), 2010 international conference on*. IEEE, 1–9.

[12] Janne Haverinen and Anssi Kemppainen. 2009. Global indoor self-localization based on the ambient magnetic field. *Robotics and Autonomous Systems* 57, 10 (2009), 1028–1035.

[13] Benjamin Kempke, Pat Pannuto, and Prabal Dutta. 2015. PolyPoint: Guiding indoor quadrotors with ultra-wideband localization. In *Proceedings of the 2nd International Workshop on Hot Topics in Wireless*. ACM, 16–20.

[14] Byunghun Kim, Myungchul Kwak, Jeongkeun Lee, and Ted Taekyoung Kwon. 2014. A multi-pronged approach for indoor positioning with WiFi, magnetic and cellular signals. In *Indoor Positioning and Indoor Navigation (IPIN), 2014 International Conference on*. IEEE, 723–726.

[15] Seong-Eun Kim, Yong Kim, Jihyun Yoon, and Eung Sun Kim. 2012. Indoor positioning system using geomagnetic anomalies for smartphones. In *Indoor Positioning and Indoor Navigation (IPIN), 2012 International Conference on*. IEEE, 1–5.

[16] Kionix. 2016. KMX62-1031 Specification rev. 3.0. http://www.kionix.com/product/KMX62-1031. (2016).

[17] Binghao Li, Thomas Gallagher, Andrew G Dempster, and Chris Rizos. 2012. How feasible is the use of magnetic field alone for indoor positioning?. In *Indoor Positioning and Indoor Navigation (IPIN), 2012 International Conference on*. IEEE, 1–9.

[18] Fan Li, Chunshui Zhao, Guanzhong Ding, Jian Gong, Chenxing Liu, and Feng Zhao. 2012. A reliable and accurate indoor localization method using phone inertial sensors. In *Proceedings of the 2012 ACM Conference on Ubiquitous Computing*. ACM, 421–430.

[19] Zhenguang Liu, Luming Zhang, Qi Liu, Yifang Yin, Li Cheng, and Roger Zimmermann. 2017. Fusion of Magnetic and Visual Sensors for Indoor Localization: Infrastructure-Free and More Effective. *IEEE Transactions on Multimedia* 19, 4 (2017), 874–888.
[20] Nesma Mohssen, Rana Momtaz, Heba Aly, and Moustafa Youssef. 2014. It's the human that matters: accurate user orientation estimation for mobile computing applications. In *Proceedings of the 11th International Conference on Mobile and Ubiquitous Systems: Computing, Networking and Services*. ICST (Institute for Computer Sciences, Social-Informatics and Telecommunications Engineering), 70–79.
[21] Nordic. 2016. nRF52832 Product Specification 1.0. https://www.nordicsemi.com/eng/Products/Bluetooth-low-energy/nRF52832. (2016).
[22] Talat Ozyagcilar. 2012. Calibrating an ecompass in the presence of hard and soft-iron interference. *Freescale Semiconductor Ltd* (2012).
[23] Karunakar Pothuganti and Anusha Chitneni. 2014. A comparative study of wireless protocols: Bluetooth, UWB, ZigBee, and Wi-Fi. *Advance in Electronic and Electric Engineering* 4, 6 (2014), 655–662.
[24] Azkario Rizky Pratama, Risanuri Hidayat, et al. 2012. Smartphone-based pedestrian dead reckoning as an indoor positioning system. In *System Engineering and Technology (ICSET), 2012 International Conference on*. IEEE, 1–6.
[25] Anshul Rai, Krishna Kant Chintalapudi, Venkata N Padmanabhan, and Rijurekha Sen. 2012. Zee: Zero-effort crowdsourcing for indoor localization. In *Proceedings of the 18th annual international conference on Mobile computing and networking*. ACM, 293–304.
[26] Yuanchao Shu, Cheng Bo, Guobin Shen, Chunshui Zhao, Liqun Li, and Feng Zhao. 2015. Magicol: Indoor localization using pervasive magnetic field and opportunistic WiFi sensing. *IEEE Journal on Selected Areas in Communications* 33, 7 (2015), 1443–1457.
[27] Yuanchao Shu, Kang G Shin, Tian He, and Jiming Chen. 2015. Last-mile navigation using smartphones. In *Proceedings of the 21st Annual International Conference on Mobile Computing and Networking*. ACM, 512–524.
[28] Matti Siekkinen, Markus Hiienkari, Jukka K Nurminen, and Johanna Nieminen. 2012. How low energy is bluetooth low energy? comparative measurements with zigbee/802.15. 4. In *Wireless Communications and Networking Conference Workshops (WCNCW)*. IEEE, 232–237.
[29] Bluetooth SIG. 2014. Bluetooth Specification version 4.2. https://www.bluetooth.org/DocMan/handlers/DownloadDoc.ashx?doc_id=286439. (2014).
[30] Bluetooth SIG. 2016. Bluetooth Specification version 5.0. https://www.bluetooth.org/DocMan/handlers/DownloadDoc.ashx?doc_id=421043&_ga=2.95164572.1071486365.1502719791-975213286.1502719791. (2016).
[31] SKT. 1997. SK Telecom Co., Ltd. http://www.sktelecom.com. (1997).
[32] Kalyan Pathapati Subbu, Brandon Gozick, and Ram Dantu. 2013. Locateme: Magnetic-fields-based indoor localization using smartphones. *ACM Transactions on Intelligent Systems and Technology (TIST)* 4, 4 (2013), 73.
[33] S Suksakulchai, S Thongchai, DM Wilkes, and K Kawamura. 2000. Mobile robot localization using an electronic compass for corridor environment. In *Systems, Man, and Cybernetics, 2000 IEEE International Conference on*, Vol. 5. IEEE, 3354–3359.
[34] Lorenzo Taponecco, AA D'amico, and Umberto Mengali. 2011. Joint TOA and AOA estimation for UWB localization applications. *IEEE Transactions on Wireless Communications* 10, 7 (2011), 2207–2217.
[35] Ilari Vallivaara, Janne Haverinen, Anssi Kemppainen, and Juha Röning. 2010. Simultaneous localization and mapping using ambient magnetic field. In *Multisensor Fusion and Integration for Intelligent Systems (MFI)*. IEEE, 14–19.
[36] Xian Wang, Paula Tarrío, Eduardo Metola, Ana Bernardos, and José Casar. 2012. Gesture recognition using mobile phone's inertial sensors. *Distributed Computing and Artificial Intelligence* (2012), 173–184.
[37] Hongwei Xie, Tao Gu, Xianping Tao, Haibo Ye, and Jian Lu. 2016. A reliability-augmented particle filter for magnetic fingerprinting based indoor localization on smartphone. *IEEE Transactions on Mobile Computing* 15, 8 (2016), 1877–1892.
[38] Hai-Bo Ye, Tao Gu, Xian-Ping Tao, and Jian Lv. 2015. Infrastructure-free floor localization through crowdsourcing. *Journal of Computer Science and Technology* 30, 6 (2015), 1249–1273.
[39] Moustafa Youssef and Ashok Agrawala. 2005. The Horus WLAN location determination system. In *Proceedings of the 3rd international conference on Mobile systems, applications, and services*. ACM, 205–218.
[40] Cemin Zhang, Michael Kuhn, Brandon Merkl, Aly E Fathy, and Mohamed Mahfouz. 2006. Accurate UWB indoor localization system utilizing time difference of arrival approach. In *Radio and Wireless Symposium, 2006*. IEEE, 515–518.
[41] Chi Zhang and Xinyu Zhang. 2016. LiTell: indoor localization using unmodified light fixtures. In *Proceedings of the 22nd Annual International Conference on Mobile Computing and Networking*. ACM, 481–482.
[42] Rui Zhang, Amir Bannoura, Fabian Höflinger, Leonhard M Reindl, and Christian Schindelhauer. 2013. Indoor localization using a smart phone. In *Sensors Applications Symposium (SAS), 2013*. IEEE, 38–42.
[43] Yiyang Zhao, Chen Qian, Liangyi Gong, Zhenhua Li, and Yunhao Liu. 2015. LMDD: Light-weight Magnetic-based Door Detection with Your Smartphone. In *Parallel Processing (ICPP), 2015 44th International Conference on*. IEEE, 919–928.
[44] Pengfei Zhou, Mo Li, and Guobin Shen. 2014. Use it free: Instantly knowing your phone attitude. In *Proceedings of the 20th annual international conference on Mobile computing and networking*. ACM, 605–616.
[45] Shilin Zhu and Xinyu Zhang. 2017. Enabling High-Precision Visible Light Localization in Today's Buildings. In *Proceedings of the 15th Annual International Conference on Mobile Systems, Applications, and Services*. ACM, 96–108.
[46] Yuan Zhuang, Jun Yang, You Li, Longning Qi, and Naser El-Sheimy. 2016. Smartphone-based indoor localization with bluetooth low energy beacons. *Sensors* 16, 5 (2016), 596.

[47] Kathryn Zickuhr. 2013. Location-based services. *Pew Research* (2013), 679–695.

Received August 2017; revised November 2018; accepted January 2018